Effects of process parameters on the microstructure and conductive properties of $LaNiO_3$ thin films

ZIYANG ZHANG[a,b], JIE XING[a,*], BIN HE[b], JIAN CAO[b], YANTING DUAN[b], ZHIYUAN ZHENG[a], ZILI ZHANG[a]
[a]*School of Science, China University of Geosciences, Beijing 100083, China*
[b]*School of Geophysics and Information Technology, China University of Geosciences, Beijing 100083, China*

Conductive films of perovskite $LaNiO_3$ (LNO) were grown on $LaAlO_3$ (LAO) and silica using radio frequency sputtering. Effects of process parameters such as annealing condition, deposition atmosphere, deposition temperature and sputtering time on the microstructure and conductive properties were investigated. Experimental analysis showed the microstructure and conductive properties of films were improved after annealing. A mixture of O_2 and Ar with ratio of 1:6 was the optimal atmosphere. It was found that the temperature to achieve minimum resistivity was 200 °C when LNO film was deposited on LAO substrate. A semiconductive property was found when sputtering time decreased down to 5 minutes. LNO films with resistivity of 3.9×10^{-4} Ω·cm was fabricated, which provided optimum electrodes for the subsequent epitaxial growth of ferroelectric thin films.

(Received November 15, 2012; accepted April 11, 2013)

Keywords: $LaNiO_3$ thin films, Microstructure, Conductive properties

1. Introduction

In recent years, much attention has been paid to ferroelectric thin films with metal-insulator transition, high-temperature superconducting, ferroelectric and ferromagnetic properties [1]. The researches show that the characteristics of ferroelectric thin films depend on their structures, so choosing an approximate electrode material with highly matched lattice is of great significance. Pt metal has been applied as electrode material in the past few years; however, it is easy to produce electricity fatigue because of its poor compatibility with substrate material. So the conductive metal oxide films ($SrRuO_3$, $LaNiO_3$) become the most promising candidate due to the advantage of decreasing the leakage current and improving the polarization fatigue of ferroelectric film materials (e.g. $BiFeO_3$, $PbTiO_3$, $Pb(Zr,Ti)O_3$) [2-4].

$LaNiO_3$ (LNO) has a pseudo-cubic perovskite structure with a lattice parameter of 0.384 nm, which is well matched with the lattice constant of many perovskite oxides [5]. And LNO thin films with no doping have a very high conductivity, which is comparable with metal. So LNO is an ideal candidate as electrode material for epitaxial growth of ferroelectric films [6]. There are lots of methods to fabricate LNO films, such as sol-gel method [7], pulsed laser deposition (PLD) [8] and magnetron sputtering [1-4, 6]. When using sol-gel method to fabricate LNO films, people can precisely control the film's stoichiometry with simple and inexpensive equipment, but it has disadvantages of weak compactness and is easy to crack after processing. PLD has been reported to produce high-quality LNO films, however, the deposition film area is limited and the cost is very expensive. Magnetron sputtering is one of the most extensively used methods for the deposition of oxide films, as it is easy to obtain large-area epitaxial films with good uniformity at a low substrate temperature. And it is of a relatively low cost, high efficiency and low energy-consuming.

In this work, we fabricate LNO thin films by magnetron sputtering. The effects of different process parameters, including deposition atmosphere, deposition time, deposition temperature, and annealing conditions, on the microstructure and conductive properties of LNO films have been investigated.

2. Experiments

LNO thin films were prepared by radio frequency magnetron sputtering JPGF-400 (13.56 MHz). The target was prepared by a conventional solid state reaction method with diameter of 60 mm and thickness of 5 mm. Substrates were firstly cleaned in acetone, alcohol and deionized water for 10 minutes in an ultrasonic container in sequence. The background vacuum was better than 5.5×10^{-3} Pa before starting up sputtering. Then the substrate was heated up to target temperature. After the temperature was stable, Ar and O_2 were introduced into the chamber controlled by a flow rate gauge. The preliminary sputtering time was 10 minutes to remove surface

contaminants of LNO target material.

A mixture of O_2 and Ar gas was introduced into the chamber and the total working pressure was kept at 2 Pa. The sputtering power was 70 W. The deposition temperature ranged from 200 °C to 600 °C. Different deposition time was applied to obtain different thickness of LNO films. After deposition, the as-sputtered LNO films were annealed in muffle furnace in the air. The structural characterizations of the films were examined by X-ray diffraction (XRD) measurements. Surface morphologies were observed by scanning electron microscopy (SEM). Temperature-dependence of resistivity was investigated using the standard DC four-point probe method.

3. Results and discussion

3.1 Effect of annealing condition

Fig. 1 shows XRD spectra of $LaNiO_3$ films deposited on LAO annealed at different conditions. The sputtering parameters are listed in Table 1. As we can see from Fig. 1, weak pseudocubic (*l*00) diffraction peaks of sample A1 appear, and the diffraction peaks from film and substrate overlap, which indicates that the LNO films are poorly crystallized with an insufficient growth. Meanwhile, for sample A3, the intensity of (*l*00) diffraction peaks becomes stronger and narrower, as is clearly shown in Fig. 1. And for sample A2, the peak intensity of films is higher than that of substrate, which indicates the oxygen-rich environment is beneficial to form better epitaxial LNO films [2].

The resistivity of sample A1 is $16\times10^{-4}\,\Omega\cdot$cm, whereas the resistivity of sample A3 becomes only $5.2\times10^{-4}\,\Omega\cdot$cm. F. Sánchez et al [9] reported that the resistivity of LNO films depends greatly on the crystallization. As we can see in Fig. 1, the crystallization of sample A3 becomes more sufficient with bigger grain size and fewer lattice defects, which results in the reduction of the scattering from impurities. The resistivity of sample A2 is $4.5\times10^{-4}\,\Omega\cdot$cm, meaning a better crystallization achieved in this sample. Concentration of oxygen vacancies could also influence electrical resistivity seriously [10]. Oxygen vacancies in sample A1 are much more than those in samples A2 and A3. And so, sample A1 has more insulating phases and higher electrical resistivity.

Table 1. Fabrication parameters of samples A1-A3.

Sample	Substrate	Deposition temperature (°C)	Deposition time (minutes)	Deposition atmosphere (O_2:Ar)	Annealing condition
A1	LAO	600	120	1:6	No annealing
A2	LAO	600	120	1:6	in-situ oxygen
A3	LAO	600	120	1:6	air

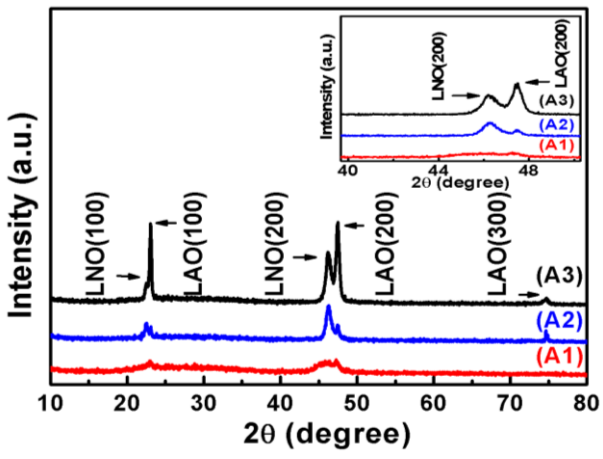

Fig. 1. XRD spectra of samples A1-A3 processed by different annealing conditions, (A1) no annealing, (A2) annealing in-situ oxygen, (A3) annealing in the air, the inset shows XRD θ-2θ spectra ranging from 40° to 50°.

3.2 Effect of deposition atmosphere

Fig. 2 shows XRD spectra of samples B1-B3 fabricated at different Ar/O ratios. The fabrication parameters are listed in Table 2. All the LNO films are grown epitaxially on LAO with obvious (*l*00) peaks. With the increase of oxygen flow, the (200) peaks of LNO become obviously higher and narrower. The lattice constant can be calculated based on Bragg's equation $2d\sin\theta=k\lambda$, where d is the lattice constant, λ is the X-ray wavelength, θ is the diffraction angle, k is an integer. And the grain size can be expressed by Scherrer's equation $D = k\lambda/B\cos\theta$, where d represents the particle size, λ is the X-ray wavelength, B is the full-width at half-maximum (FWHM) of the x-ray diffraction peak, θ is the diffraction angle, and k is the Scherrer constant and was set as 0.89 here. The calculated parameters are listed in Table 3. The evolutions of crystallization for LNO films at three growth atmospheres are clearly demonstrated in Fig. 3. A decrease

of FWHM is observed, which can be due to an increase of grain size and decrease of defects. As oxygen flow increases, the lattice constant of films changes from 0.391 nm to 0.395 nm. And the lattice constants of all the three samples are higher than LNO bulk lattice constant 0.384 nm.

The inset of Fig. 2 shows the electrical resistivities of samples B1-B3. As we can see, with the increase of oxygen flow, the electrical resistivity initially decreases quickly but then increases, which is similar to the result reported by L. H. Yang et al [11]. Under the low oxygen partial pressure, more oxygen vacancies are introduced into the film, which results in the conductive LNO decomposing into insulating La_2NiO_4. The reaction is given by the following equation

$$2LaNiO_3 \rightarrow LaNiO_4 + NiO + 1/2O_2. \quad (1)$$

As the oxygen partial pressure increases, oxygen vacancies are reduced and Ni^{2+} converts into Ni^{3+}, which is expressed as the following equation

$$2Ni^{2+} + O \rightarrow 2Ni^{3+} + O^{2-}. \quad (2)$$

The energy levels of $2p^6$-O and $3d^8$-Ni overlap, resulting in conductive $LaNiO_3$ films [12]. However, if the oxygen partial pressure is higher than 1:6, the resistivity tends to increase. This may be due to the deteriorative crystal quality caused by the higher oxygen flow.

Table 2. Fabrication parameters of samples B1-B3.

Sample	Substrate	Deposition temperature (°C)	Deposition time (minutes)	Deposition atmosphere (O_2:Ar)	Annealing condition
B1	LAO	600	60	0	air
B2	LAO	600	60	1:6	air
B3	LAO	600	60	1:3	air

Table 3. Characteristic parameters of samples B1-B3 fabricated at different deposition atmospheres.

Sample	The strongest Peak	2θ (degree)	FWHM (degree)	Lattice constant (nm)	Grain size (nm)
B1	(200)	46.388	1.22	0.391	7.0869
B2	(200)	46.187	0.86	0.392	10.0467
B3	(200)	45.906	0.62	0.395	13.9203

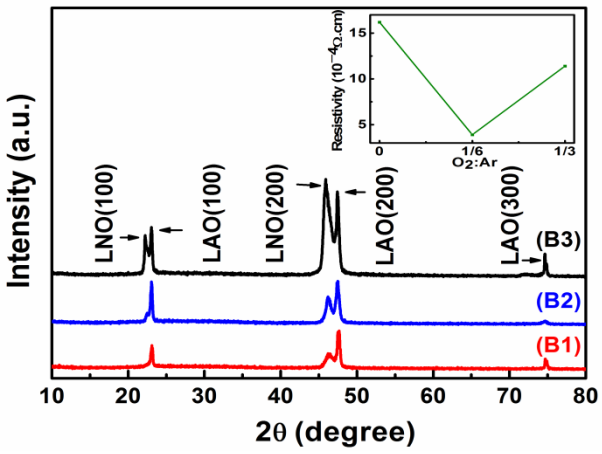

Fig. 2. XRD spectra of samples B1-B3 deposited under different deposition atmospheres, (B1) O_2:Ar=0, (B2) O_2:Ar=1:6, (B3) O_2:Ar=1:3. The inset shows evolution of the electrical resistivity of samples B1-B3.

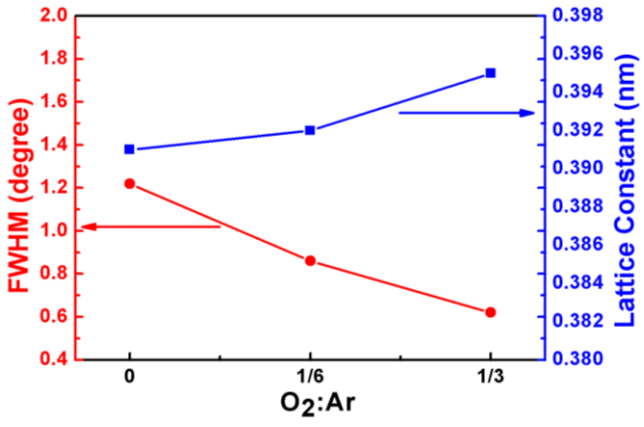

Fig. 3. Evolutions of full-width at half-maximum (FWHM) and lattice constant for samples B1-B3.

3.3 Effect of deposition temperature

Fig. 4 shows XRD spectra of samples C1-C3 deposited at different temperatures. The sputtering parameters are listed in Table 4. As deposition temperature increases, the (200) diffraction peaks shift to lower diffraction angles, which indicates the lattice constant is becoming larger. We can also note that the intensity of diffraction peaks becomes stronger as deposition temperature increases [13]. The inset of Fig. 4 shows evolution of the electrical resistivity of samples C1-C3. The resistivity gradually increases with the deposition temperature, and the lowest resistivity of LNO films is $3.9\times10^{-4}\,\Omega\cdot$cm, which has qualified the requirements as the electrode material [14]. We obtained the conductive LNO films at a quite low temperature, which is very favorable for the fabrication of thin films device.

Table 4. Fabrication parameters of samples C1-C3.

Sample	Substrate	Deposition temperature (°C)	Deposition time (minutes)	Deposition atmosphere (O_2:Ar)	Annealing condition
C1	LAO	600	60	1:6	air
C2	LAO	400	60	1:6	air
C3	LAO	200	60	1:6	air

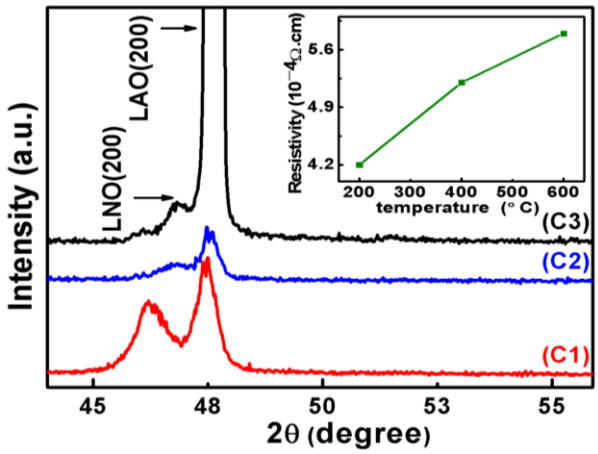

Fig. 4. XRD spectra of samples C1-C3 deposited at different temperatures, (C1) 600°C, (C2) 400°C, (C3) 200°C. The inset shows evolution of resistivity of samples C1-C3.

3.4 Effect of deposition time

XRD spectra of samples DL1-5 and DS1-5 with different deposition time are shown in Fig. 5. The sputtering parameters are listed in Table 5. All films are identified to be pseudocubic perovskite structure, of which strong (100) and (200) diffraction peaks can be observed. The intensity of the diffraction peaks become stronger as the deposition time increases, which indicates that the crystallization becomes better. Fig. 6 shows SEM pictures of LNO films deposited on silica and LAO for different time. The surfaces of all the films are smooth, uniform without cracks and pinholes. With the deposition time increasing, the grains obviously grow bigger and are closely packed, which is agreed with the XRD result.

Fig. 7 shows deposition time dependence of the electrical resistivity of samples DL1-5 and DS1-5. The resistivity of sample DS1 deposited on silica for 5 minutes is high, and then with the deposition time increasing, the resistivity reduces rapidly. But the change is not so obvious when deposition time is over 30 minutes. Meanwhile, the resistivities of samples DL1-5 deposited on LAO are relatively low and the change tendency with time is not so evident as deposited on silica. From the perspective of the films growth dynamics, we understand the process as the following. When the few LNO atoms are deposited on the substrate, they will initially form a transition layer on substrate surface. The LNO films are amorphous and have many defects, which leads to a poor conductivity. As deposition time increases, the LNO atoms will overcome the influence of the disorder from the bottom amorphous layer, achieving a better crystallization and lower resistivity.

To further investigate the conductive mechanism and transport properties of LNO films, temperature dependence of resistivity measurements are carried out. Fig. 8 shows temperature dependence of resistance of samples DL1-3 in a semi-logarithmic scale. The films deposited for 10 and 30 minutes exhibit a metallic conduction behavior from 40 to 300 K. While for the film deposited for 5 minutes, the resistivity exhibits a decrease tendency with the increase of temperature, which indicates a semiconductive transport mechanism in the film. The nature of the semiconductive transport mechanism can be explained as follows. The oxygen vacancies are rich near the interface between film and the substrate. When the deposition time decreases to 5 minutes, the film is very thin and the relative fraction of nonstoichiometric part increases, which results a semiconductive transport mechanism [15]. However, further studies should be necessary to draw firm explanation on this point.

Table 5. Fabrication parameters of samples DL1-5 and DS1-5.

Sample	Substrate	Deposition temperature (°C)	Deposition time (minutes)	Deposition atmosphere (O_2:Ar)	Annealing atmosphere
DL1	LAO	600	5	1:6	air
DL2	LAO	600	10	1:6	air
DL3	LAO	600	30	1:6	air
DL4	LAO	600	60	1:6	air
DL5	LAO	600	120	1:6	air
DS1	silica	600	5	1:6	air
DS2	silica	600	10	1:6	air
DS3	silica	600	30	1:6	air
DS4	silica	600	60	1:6	air
DS5	silica	600	120	1:6	air

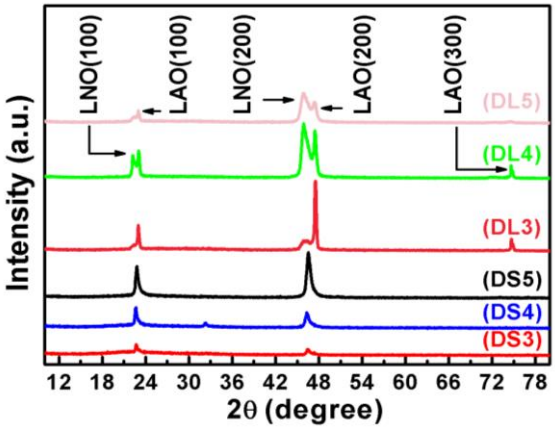

Fig. 5. XRD spectra of samples DS3-5 and DL3-5 with different deposition time, (DS3) 30 minutes deposited on silica, (DS4) 60 minutes deposited on silica, (DS5) 120 minutes deposited on silica, (DL3) 30 minutes deposited on LAO, (DL4) 60 minutes deposited on LAO, (DL5) 120 minutes deposited on LAO.

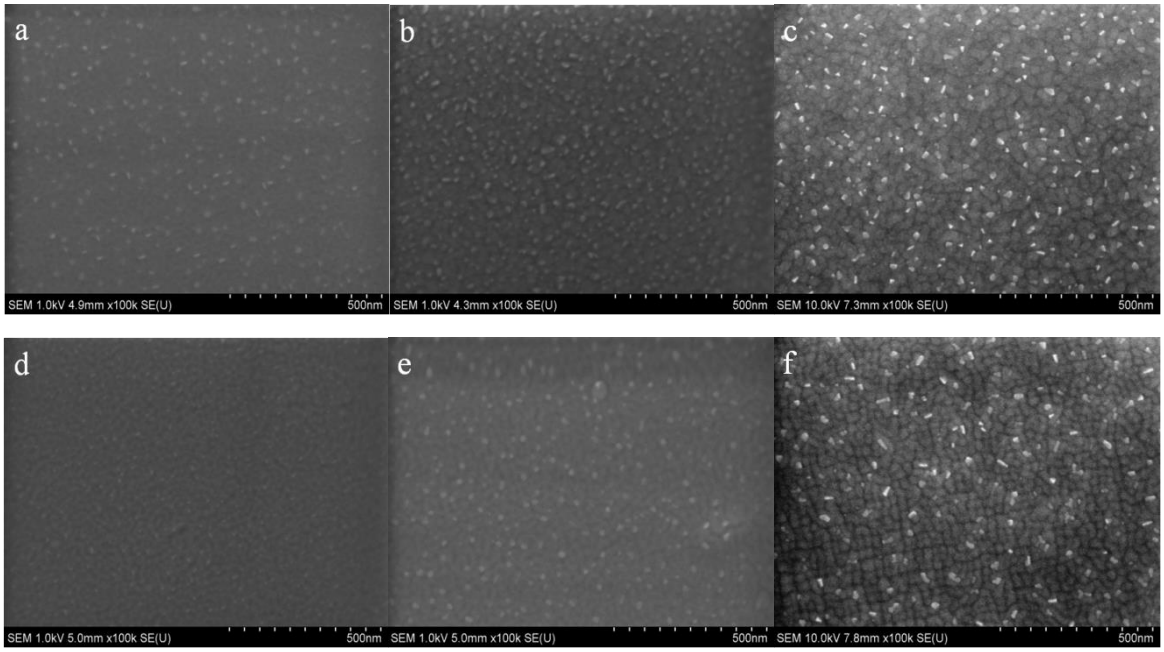

Fig. 6. SEM micrographs of samples DS3-5 and DL3-5 with different deposition time, (a) 30 minutes deposited on silica, (b) 60 minutes deposited on silica, (c) 120 minutes deposited on silica, (d) 30 minutes deposited on LAO, (e) 60 minutes deposited on LAO, (f) 120 minutes deposited on LAO.

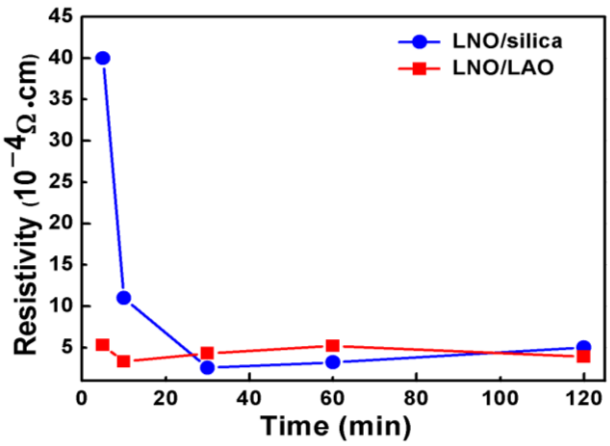

Fig. 7. Evolutions of the electrical resistivity of samples DS1-5 and DL1-5 with different deposition time.

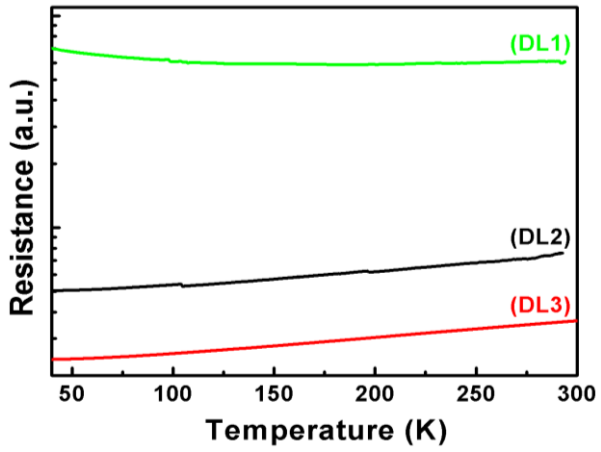

Fig. 8. Resistance of samples DL1-3 versus temperature in a semi-logarithmic scale, (DL1) 5 minutes, (DL2) 10 minutes, (DL3) 30 minutes.

4. Summary

Conductive $LaNiO_3$ films were deposited on $LaAlO_3$ and silica substrate by magnetron sputtering respectively. We studied effects of process parameters on the microstructure and conductive properties of LNO thin films by varying annealing condition, deposition atmosphere, deposition temperature and deposition time. The microstructure and conductive properties of LNO films annealing in-situ oxygen atmosphere were better than those annealing in the air, and the $LaNiO_3$ films with no annealing had the worst conductivity. Increasing the oxygen partial pressure could improve characteristics of LNO films to a degree, but too high oxygen partial pressure would cause a decline in the resistivity of films. For the LNO films grown on LAO, the optimal deposition temperature was 200 °C, and the resistivity increased with deposition temperature. We found an amorphous transition layer was formed at the initial stage of growth. The LNO films showed a semiconductive property as the deposition time decreased down to 5 minutes when deposited on LAO. The LNO films with resistivity of $3.9\times10^{-4}\,\Omega\cdot$cm has been fabricated, which is a good candidate for integrating ferroelectric capacitors.

Acknowledgements

This work was financially supported by National Natural Science Foundation of China (Grant No. 11104255), Fundamental Research Funds for the Central Universities (Grant Nos. 2010ZY50 and 2011YYL006).

References

[1] L. Qiao, X. F. Bi, Journal of Crystal Growth, **3653**, 310 (2008).
[2] M. Detalle, D. Rémiens, Journal of Crystal Growth, **3596**, 310 (2008).
[3] L. H. Yang, G. S. Wang, C. L. Mao, Y. Y. Zhang, R. H. Liang, C. Soyer, D. Rémiens, X. L. Dong, Journal of Crystal Growth, **4241**, 311 (2009).
[4] X. D. Zhang, X. J. Meng, J. L. Sun, T. Lin, J. H. Ma, J. H. Chu, D. Y. Kwon, C. W. Kim, B. G. Kim, The Solid Films, **919**, 516 (2008).
[5] K. Ueno, T. Yamaguchi, W. Sakamoto, T. Yogo, K. Kikuta, S. Hirano, Thin Solid Films, **78**, 491 (2005).
[6] C. Wang, M. H. Kryder, Physical Scripta, **035601**, 78 (2008).
[7] N. Yin, H. C. Wang, C. L. Wang, Journal of Rare Earths, **506**, 27 (2009).
[8] T. Yu, Y. F. Chen, Z. G. Liu, X. Y. Chen, L. Sun, N. B. Minutesg, L. J. Shi, Materials Letters, **73**, 26 (1996).
[9] F. Sánchez, C. Ferrater, C. Guerrero, M. V. García-Cuenca, M. Varela, Applied Physics A: Materials Science and Processing, **59**, 71 (2000).
[10] R. D. Sánchez, M. T. Causa, A. Caneiro, A. Butera, M. Vallet-Regí, M. J. Sayagués, J. González-Calbet, F. García-Sanz, J. Rivas: Phys. Rev. B, **16574**, 54 (1996).
[11] L. H. Yang, G. S. Wang, C. L. Mao, Y. Y. Zhang, R. H. Liang, C. Soyer, D. Rémiens, X. L. Dong, Journal of Crystal Growth, **4241**, 311 (2009).
[12] J. B. Torrance, P. Lacorre, A. I. Nazzal, E. J. Ansaldo, C. Niedermayer: Phys. Rev. B, **8209**, 45 (1992).
[13] C. C. Zhang, J. Hou, R. Rao, C.S. Yang, G. F. Ding, Thin Solid Films, **6837**, 517 (2009).
[14] Y. Wang, G. F. Zhang, C. S. Li, G. Yan, Y. F. Lu, Bulletin of Materials Science, **1379**, 34 (2011).
[15] R. Scherwitzl, S. Gariglio, M. Gabay, P. Zubko, M. Gibert, J. M. Triscone: Physical Review Letters, **246403**, 106 (2011).

*Corresponding author: jxing2011@gmail.com